Received: 15 September 2020 | Revised: 20 November 2020 | Accepted: 14 December 2020

DOI: 10.1002/htj.22045

RESEARCH ARTICLE

HEAT TRANSFER WILEY

Statistical analysis on three-dimensional MHD convective Carreau nanofluid flow due to bilateral nonlinear stretching sheet with heat source and zero mass flux condition

Alappat Sunny Sabu | **Sujesh Areekara** | **Alphonsa Mathew**

Department of Mathematics, St. Thomas' College (Autonomous), Thrissur, Kerala, India

Correspondence
Alphonsa Mathew, Department of Mathematics, St. Thomas' College (Autonomous), Thrissur-680001, Kerala, India.
Email: alphonsa@stthomas.ac.in

Abstract

This study focuses on analyzing the response of a magnetohydrodynamic convective Carreau nanofluid flow over a bilateral nonlinear stretching sheet in the presence of a heat source and zero mass flux condition. The problem has been solved numerically using the MATLAB built-in function bvp5c. The findings of velocity, temperature, and concentration profiles based on the various parameters are illustrated using graphs. The impact of various parameters on the heat transfer rate is scrutinized using statistical techniques, like, correlation coefficient, probable error, and regression. The effect of various parameters on skin friction coefficients is studied via tables and slope of linear regression. It is observed that the statistical results coincide with the numerical results. It is also noticed that the stretching ratio parameter increases the *Y*-directional velocity profile. Accuracy of the numerical procedure has been validated through a restrictive comparison of the present work with previous published results and is found to be in good agreement.

KEYWORDS

bilateral nonlinear stretching sheet, Carreau nanofluid, heat source, MHD flow, regression analysis, zero mass flux

1 | INTRODUCTION

The natural convection magnetohydrodynamic (MHD) flow has been studied by many researchers theoretically and experimentally, and it has applications in scientific, engineering, and medical fields. It plays a pivotal role in the field of microelectronics, solar technology, glass fibers, hot rolling, paper production, and plasma studies.[1–3] Naga et al.[4] studied magneto Carreau nanofluid numerically under slip condition and obtained suppressed velocity profiles through augmented values of the Hartmann number. Abbas et al.[5] analyzed the MHD flow on a stretching sheet using Carreau fluid. They deployed a Runge–Kutta fourth-order method for solving the problem numerically.

Among the seven slip mechanisms introduced by Buongiorno, Brownian motion and thermophoresis effects are of great importance. Goudarzi et al.[6] investigated the impact of thermophoresis and Brownian motion due to the natural convection on hybrid Ag–MgO water nanofluid. They found out that the Nusselt number increases due to thermophoresis diffusion. Sardar et al.[7] investigated the Carreau nanofluid in the presence of thermophoresis and Brownian motion over a wedge. They observed a reduction in the Nusselt number due to an enhancement in the Brownian motion parameter. Hayat et al.[8] studied the effects of thermophoresis and the Brownian motion of Carreau nanofluid under Newtonian conditions using homotopy analysis method (HAM). Iqbal et al.[9] investigated the thin-film Carreau nanofluid flow on a stretching surface and observed an increased profile due to the thermophoresis parameter.

The stretched surface has intrigued many researchers due to its diverse applications in industrial and engineering fields, like, production of plastic and rubber plates, cooling of metallic plate in a bath, metal extrusion, and so forth. Khan et al.[10] studied the heat transfer over a bilateral stretched nonlinear surface numerically with the aid of optimal homotopy asymptotic method (OHAM) and Runge–Kutta coupled with shooting method. Hussain et al.[11] analyzed the effect of heat generation of carbon nanotubes (CNTs) nanofluids over a nonlinear bilateral stretched surface. A reduced thermal layer due to the rate of stretching was noted. Nandeppanavar and Siddalingappa[12] analyzed the consequence of thermal radiation and viscous dissipation on heat transfer over a nonlinear stretching sheet through a porous medium, and they inferred a positive and negative effect on temperature due to the Eckert number and thermal radiation parameter, respectively. Tlili et al.[13] investigated the three-dimensional flow over a stretched surface using the Williamson fluid, and they established that the velocity along the Y-direction enhanced due to stretching. Hayat et al.[14] investigated the Carreau nanofluid flow induced by a bilateral stretched surface. They tackled the nonlinear differential equations using NDsolve. Shakunthala and Nandeppanavar[15] studied the boundary layer flow and Cattaneo–Christov heat flux of a nonlinear stretching sheet with suspended CNTs.

Patel and Singh[16] studied the micropolar fluid over a stretched sheet with convective boundary conditions in the presence of Brownian motion and thermophoresis effects. An improvement in heat transfer due to increased Biot numbers was observed. Tlili et al.[17] carried out numerical investigations on the MHD flow, heat and mass transfer, and rate of entropy generation over a wedge. Nayak et al.[18] studied the combined effects of slip and convective boundary condition on the MHD three-dimensional stretched flow of a nanofluid through porous media under nonlinear thermal radiation. Ray et al.[19] studied the nonsimilar solution of the Eyring–Powell fluid flow and heat transfer with the convective boundary condition using HAM.

Mass flux corresponds to the rate of mass flow per unit area perpendicular to the direction of flow. Zero mass flux[20,21] is the condition when the normal flux of nanoparticles is zero at the boundary. Ramzan et al.[22] examined the flow of couple stress nanofluid past an exponential stretched surface and observed that for growing values of Brownian motion and thermophoresis parameters, the concentration profile exhibits decreasing and increasing behavior, respectively. Uddin et al.[23] investigated the impact of buoyancy forces on the stagnation point flow of magneto-nanoparticles under zero mass flux condition. Characteristics of a thermally stratified flow of a Sutterby nanofluid along with zero mass flux condition were analyzed by Saif-ur-Rehman et al.[24]

Hayat et al.[25] numerically studied the flow of the Carreau–Yasuda nanofluid in the presence of mixed convection and Hall current, and they observed an inverse effect for concentration profiles under thermophoresis and Brownian motion parameters. Khan et al.[26] investigated the unsteady slip flow of a Carreau nanofluid over a wedge. Nandeppanavar et al.[27] scrutinized the Carreau nanofluid flow over an exponentially stretching sheet in a saturated porous medium using the fourth-order Runge–Kutta shooting method. Khan et al.[28] numerically analyzed the Carreau fluid flow for generalized Fourier's and Fick's laws. They observed that the horizontal velocity enhances with an increase in wall thickness parameter, power-law index, Weissenberg number, thermal Grashof parameter, and bioconvection Rayleigh number.

The flow of Newtonian and non-Newtonian fluids over a bilateral nonlinear stretching sheet has been studied[10,11,13,14] in the literature. However, the MHD Carreau nanofluid flow over a bilateral stretching nonlinear surface with zero mass flux condition has not been a subject of study till date. This study makes an effort to fill this gap. In this paper, magnetic and heat source effects are accounted to analyze the effects of velocity and heat transport of Carreau nanofluid over a nonlinear stretching sheet. To increase the novelty of the present work, effects of various parameters on skin friction coefficients and heat transfer rate are scrutinized using statistical techniques,[29–31] like, slope of linear regression, correlation coefficient, probable error, and regression.

2 | MATHEMATICAL FORMULATION

Here, a three-dimensional, steady MHD Carreau nanofluid flow due to a bilateral stretching sheet with velocities $u_W = a(x+y)^m, v_W = b(x+y)^m, a, b, m > 0$ along the X- and Y-directions, respectively, is considered. Velocity, temperature, and concentration equations are investigated with convective and zero mass flux condition at the surface. A nonuniform magnetic field $B = B_0(x+y)^{\frac{m-1}{2}}$ is applied along the Z-direction (see Figure 1). In addition, a nonuniform heat generation\absorption $Q = Q_0(x+y)^{m-1}$ is implemented. The boundary layer equations[10,14,32] are given by the following:

$$u_x + v_y + w_z = 0, \tag{1}$$

$$uu_x + vu_y + wu_z = \nu_f u_{zz}\left[\beta^* + (1-\beta^*)\{1+\Gamma^2(u_z)^2\}^{\frac{n-1}{2}}\right] + \nu_f(n-1)(1 - \beta^*)\Gamma^2 u_{zz}(u_z)^2\{1+\Gamma^2(u_z)^2\}^{\frac{n-3}{2}} - \frac{\sigma B^2 u}{\rho}, \tag{2}$$

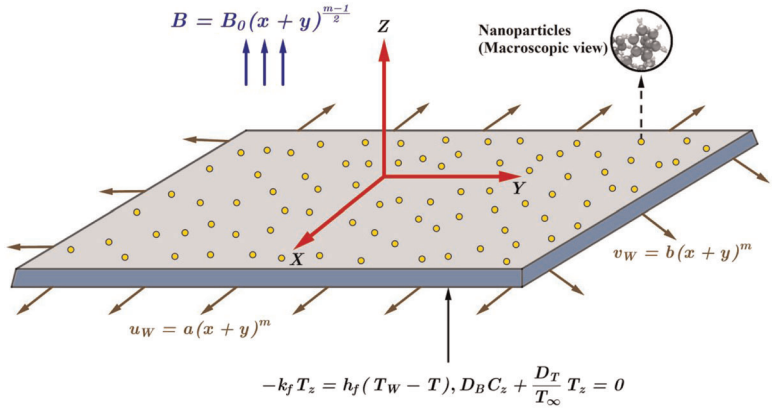

FIGURE 1 Geometry of the problem [Color figure can be viewed at wileyonlinelibrary.com]

$$uv_x + vv_y + wv_z = \nu_f v_{zz}\left[\beta^* + (1-\beta^*)\{1+\Gamma^2(v_z)^2\}^{\frac{n-1}{2}}\right] + \nu_f(n-1)(1 - \beta^*)\Gamma^2 v_{zz}(v_z)^2\{1+\Gamma^2(v_z)^2\}^{\frac{n-3}{2}} - \frac{\sigma B^2 v}{\rho}, \tag{3}$$

$$uT_x + vT_y + wT_z = \alpha_f T_{zz} + \frac{Q}{(\rho c)_f}(T - T_\infty) + \tau\left[D_B T_z C_z + \frac{D_T}{T_\infty}(T_z)^2\right], \tag{4}$$

$$uC_x + vC_y + wC_z = D_B C_{zz} + \frac{D_T}{T_\infty} T_{zz}. \tag{5}$$

The respective boundary conditions are given as follows:

$$\left.\begin{aligned} &u = u_W = a(x+y)^m, \quad v = v_W = b(x+y)^m, \quad w = 0, \\ &-k_f T_z = h_f(T_W - T), \quad D_B C_z + \tfrac{D_T}{T_\infty} T_z = 0, \end{aligned}\right\} \quad \text{at } z = 0, \tag{6}$$

$$u \to 0, \quad v \to 0, \quad T \to T_\infty, \quad C \to C_\infty \text{ as } z \to \infty. \tag{7}$$

The following similarity variables are implemented in converting the above system of partial differential equations into a system of ordinary differential equations:

$$\left.\begin{aligned} &u = a(x+y)^m f'(\zeta), \\ &v = a(x+y)^m g'(\zeta), \\ &w = -\sqrt{a\nu_f}(x+y)^{\frac{m-1}{2}}\left[\frac{m+1}{2}(f(\zeta)+g(\zeta)) + \frac{m-1}{2}\zeta(f'(\zeta)+g'(\zeta))\right], \end{aligned}\right\} \tag{8}$$

$$\theta(\zeta) = \frac{T - T_\infty}{T_W - T_\infty}, \quad \phi(\zeta) = \frac{C - C_\infty}{C_\infty}, \quad \zeta = \sqrt{\frac{a}{\nu_f}} z(x+y)^{\frac{m-1}{2}}. \tag{9}$$

The transformed boundary layer equations are given as follows:

$$f'''\left[\beta^* + (1-\beta^*)(1 + We^2(f'')^2)^{\frac{n-3}{2}}(1 + nWe^2(f'')^2)\right] - Mf' - m(f')^2 - mf'g' + \frac{m+1}{2} f''(f+g) = 0, \tag{10}$$

$$g'''\left[\beta^* + (1-\beta^*)(1+We^2(g'')^2)^{\frac{n-3}{2}}(1+nWe^2(g'')^2)\right] - Mg' - m(g')^2 - mf'g' + \frac{m+1}{2}g''(f+g) = 0, \tag{11}$$

$$\theta'' + Pr\left[S\theta + Nb\phi'\theta' + Nt(\theta')^2 + \left(\frac{m+1}{2}\right)(f+g)\theta'\right] = 0, \tag{12}$$

$$\phi'' + \frac{Nt}{Nb}\theta'' + Sc\phi'\left(\frac{m+1}{2}\right)(f+g) = 0. \tag{13}$$

The corresponding boundary conditions are given by the following:

$$\begin{aligned} f(0) = 0, g(0) = 0, \quad f'(0) = 1, g'(0) = \delta, \\ \theta'(0) = -\gamma(1-\theta(0)), \quad \phi'(0) + \frac{Nt}{Nb}\theta'(0) = 0, \end{aligned} \tag{14}$$

$$f'(\infty) \to 0, \quad g'(\infty) \to 0, \quad \theta(\infty) \to 0, \quad \phi(\infty) \to 0, \tag{15}$$

where the nondimensional parameters are taken as follows:

$$\begin{aligned} We = \sqrt{\frac{\Gamma^2 a^3 (x+y)^{3m-1}}{\gamma}}, \quad M = \frac{\sigma B_0^2}{\rho_f a}, \quad Pr = \frac{\nu_f}{\alpha_f}, \quad Sc = \frac{\nu_f}{D_B}, \delta = \frac{b}{a}, \\ Nt = \frac{\tau D_T (T_W - T_\infty)}{T_\infty \nu_f}, \quad Nb = \frac{\tau D_B C_\infty}{\nu_f}, \quad \tau = \frac{(\rho c)_p}{(\rho c)_f}, \quad S = \frac{Q_0}{a(\rho c)_f}. \end{aligned} \tag{16}$$

Skin friction coefficients, local Nusselt number, and local Sherwood number measure the surface drag, heat transfer rate, and mass transfer rate, respectively. They are defined[32,33] as follows:

Local Nusselt number	$Nu = \frac{(x+y)q_w}{k_f(T_w - T_\infty)}$, where $q_w = -k_f\left(\frac{\partial T}{\partial z}\right)_{z=0}$
Reduced form of Nusselt number	$Re_x^{-\frac{1}{2}} Nu = -\theta'(0)$, where $Re_x = \frac{u_w(x+y)}{\nu_f}$ is the local Reynolds number along the x-direction
Local Sherwood number (Sh)	$Sh = \frac{(x+y)m_w}{D_B(C_w - C_\infty)}$, where $m_w = -D_B\left(\frac{\partial C}{\partial z}\right)_{z=0}$
Reduced form of Sh	$Re_x^{-\frac{1}{2}} Sh = -\phi'(0)$
Skin friction coefficients	$Cf_x = \frac{\tau_{zx}}{\rho_f u_w^2}$, where $\tau_{zx} = \mu_f\left(\frac{\partial u}{\partial z}\right)\left[\beta^* + (1-\beta^*)\left(1+\Gamma^2\left(\frac{\partial u}{\partial z}\right)^2\right)^{\frac{n-1}{2}}\right]$ $Cf_y = \frac{\tau_{zy}}{\rho_f v_w^2}$, where $\tau_{zy} = \mu_f\left(\frac{\partial v}{\partial z}\right)\left[\beta^* + (1-\beta^*)\left(1+\Gamma^2\left(\frac{\partial v}{\partial z}\right)^2\right)^{\frac{n-1}{2}}\right]$
Reduced form of skin friction	$Re_x^{\frac{1}{2}} Cf_x = f''(0)\left[\beta^* + (1-\beta^*)(1+We^2(f''(0))^2)^{\frac{n-1}{2}}\right]$, $Re_y^{\frac{1}{2}} Cf_y = \delta^{-1.5} g''(0)\left[\beta^* + (1-\beta^*)(1+We^2(g''(0))^2)^{\frac{n-1}{2}}\right]$, where $Re_y = \frac{v_w(x+y)}{\nu_f}$ is the local Reynolds number along the y-direction

3 | NUMERICAL SOLUTION

Equations (10)–(13) with boundary conditions (14) and (15) are solved numerically using bvp5c solver, a MATLAB built-in function. To accomplish this, we consider

$$f = y_1, \quad f' = y_2, \quad f'' = y_3, \quad g = y_4, \quad g' = y_5,$$
$$g'' = y_6, \quad \theta = y_7, \quad \theta' = y_8, \quad \phi = y_9, \quad \phi' = y_{10}.$$

Accordingly, Equations (10)–(15) take the form

$$y'_1 = y_2, \quad y'_2 = y_3, \quad y'_3 = \frac{my_2^2 + my_2y_5 - \left(\frac{m+1}{2}\right)y_3\left(y_1 + y_4\right) + My_2}{\beta^* + \left(1-\beta^*\right)\left(1 + We^2y_3^2\right)^{\frac{n-3}{2}}\left(1 + nWe^2y_3^2\right)},$$

$$y'_4 = y_5, \quad y'_5 = y_6, \quad y'_6 = \frac{my_5^2 + my_2y_5 - \left(\frac{m+1}{2}\right)y_6\left(y_1 + y_4\right) + My_5}{\beta^* + \left(1-\beta^*\right)\left(1 + We^2y_6^2\right)^{\frac{n-3}{2}}\left(1 + nWe^2y_6^2\right)},$$

$$y'_7 = y_8, \quad y'_8 = -Pr\left[Sy_7 + Nby_8y_{10} + Nt(y_8)^2 + \left(\frac{m+1}{2}\right)(y_1 + y_4)y_8\right], \quad y'_9 = y_{10},$$

$$y'_{10} = \left\{\frac{Nt}{Nb}Pr\left[Sy_7 + Nby_8y_{10} + Nt(y_8)^2 + \left(\frac{m+1}{2}\right)(y_1 + y_4)y_8\right] - Scy_{10}\left(\frac{m+1}{2}\right)(y_1 + y_4)\right\},$$

$$y_1(0) = 0, y_2(0) = 1, y_2(\infty) = 0, y_4(0) = 0, y_5(0) = \delta, y_5(\infty) = 0,$$
$$y_7(\infty) = 0, \quad y_8(0) = -\gamma(1 - y_7(0)), \quad y_9(\infty) = 0, \quad y_{10}(0) + \frac{Nt}{Nb}y_8(0) = 0.$$

Accuracy of the code and the validation of the current problem has been accounted through a restrictive comparison of the present work with previous published[10] results and is found to be in good agreement (described in Table 1).

4 | RESULT AND DISCUSSION

The impact of viscosity ratio parameter (β^*), Weisssenberg number (We), Hartmann number (M), heat generation/absorption parameter (S), power-law index (n), Biot number (γ), stretching ratio parameter (δ), Brownian motion parameter (Nb), and thermophoresis

TABLE 1 Comparison of $f''(0)$ and $g''(0)$ when $\beta^* = 1$ and $M = 0$

m	δ	$f''(0)$ (present paper)	$f''(0)$[10]	$g''(0)$ (present paper)	$g''(0)$[10]
1	0	−1.000172394	−1	0	0
1	0.5	−1.22478775	−1.224745	−0.612393875	−0.612372
1	1	−1.414226121	−1.414214	−1.414226121	−1.414214
3	0	−1.624368157	−1.624356	0	0
3	0.5	−1.989423631	−1.989422	−0.994711816	−0.994711
3	1	−2.297186414	−2.297186	−2.297186414	−2.297186

parameter (Nt) on the X-direction velocity ($f'(\zeta)$), Y-direction velocity ($g'(\zeta)$), temperature ($\theta(\zeta)$), and concentration ($\phi(\zeta)$) profiles is carefully analyzed through Figures 2–10. The Prandtl number (Pr) and Schmidt numbers (Sc) are fixed at 5 and 2, respectively.

Figure 2A and 2B depicts the variation of $f'(\zeta)$ and $g'(\zeta)$ due to the increments in β^*. The analysis has been carried out for shear-thinning ($n < 1$) and shear-thickening ($n > 1$) cases. Both $f'(\zeta)$ and $g'(\zeta)$ exhibit an increase (shear-thinning case) with an increase in β^*, whereas the results are reversed for the shear-thickening case. The effect of We on $f'(\zeta)$ and $g'(\zeta)$ is elucidated in Figure 3A and 3B. A contrasting behavior is observed on the velocity profiles for different values of n. An increase in We improves the elastic forces, which hence causes a reduction in the velocity profiles in a shear-thinning fluid. Figure 4A and 4B illustrates the impact of variation of M on $f'(\zeta)$ and $g'(\zeta)$. An increment in M generates the Lorentz force, which retards $f'(\zeta)$ and $g'(\zeta)$ profiles. Figure 5 exhibits the influence of δ on $g'(\zeta)$. With an increase in δ, $g'(\zeta)$ also increases, as the vertical downward flow is accelerated due to the bidirectional stretching of the sheet.

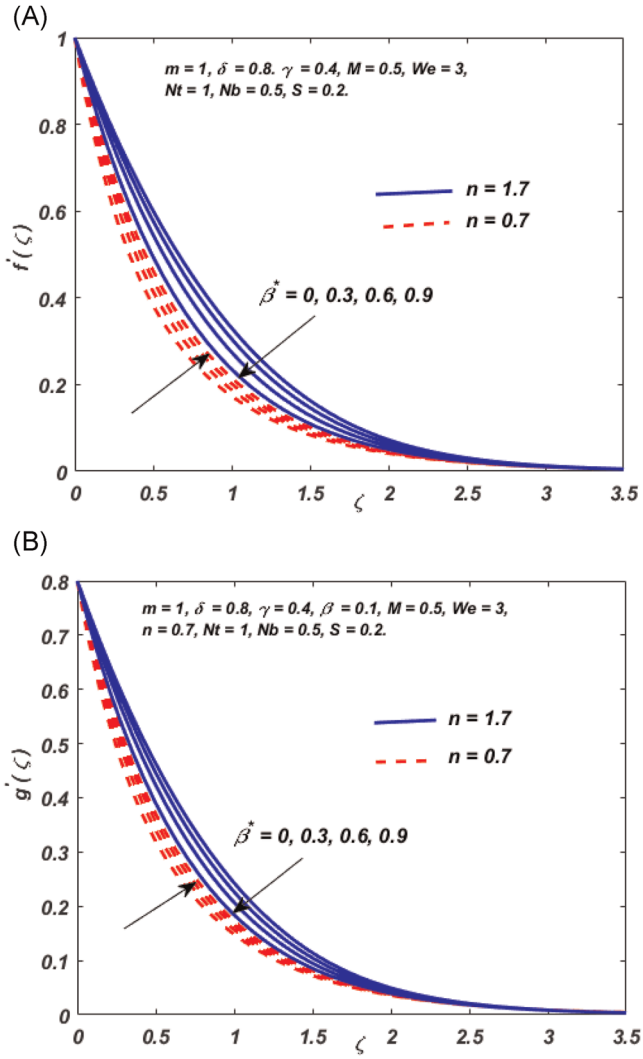

FIGURE 2 (A) Variation of $f'(\zeta)$ for various values of β^* and (B) variation of $g'(\zeta)$ for various values of β^* [Color figure can be viewed at wileyonlinelibrary.com]

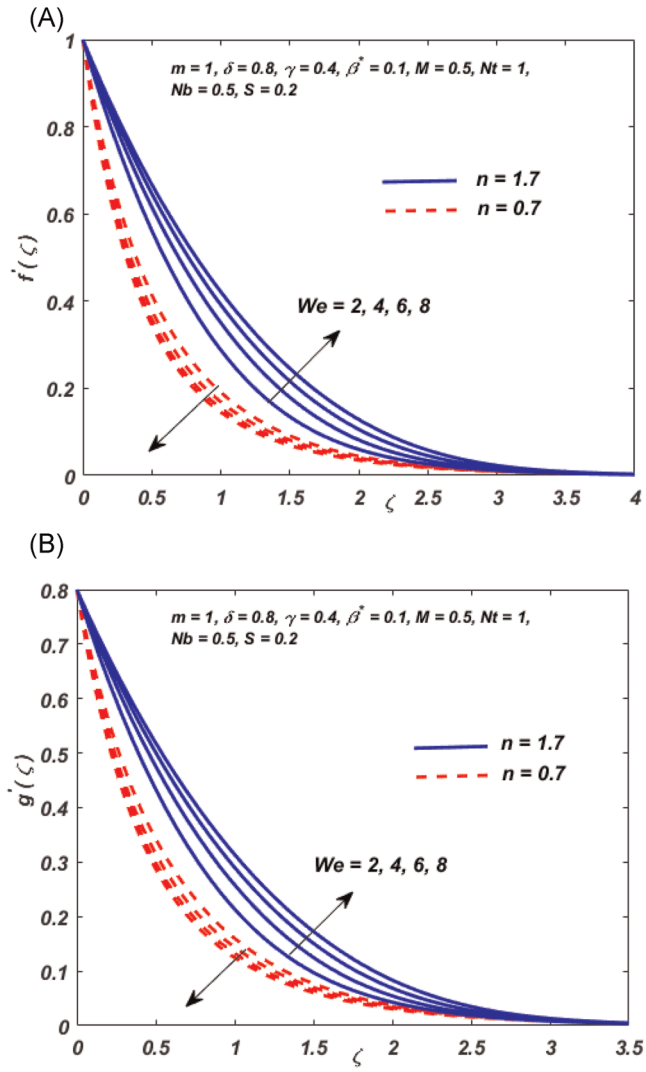

FIGURE 3 (A) Variation of $f'(\zeta)$ for various values of We and (B) variation of $g'(\zeta)$ for various values of We [Color figure can be viewed at wileyonlinelibrary.com]

With a rise in the magnitude of γ, the temperature profile is enhanced, as shown in Figure 6. Physically, this can be attributed to the fact that an increase in the Biot number enhances the heat transfer coefficient, which, in turn, increases θ. Figure 7 displays the effect of S on $\theta(\zeta)$. $\theta(\zeta)$ is observed to increase as S is increased. Figure 8 reveals the change in $\theta(\zeta)$ with an increase in Nt. Nt is found to have a positive effect. The mounting of Nt promotes an increment in the thermophoresis force, which enforces the movement of nanoparticles from a hot region to a cold region, and hence $\theta(\zeta)$ is increased. Figure 9 describes the variation of $\phi(\zeta)$ with Nb. Nb shows a negative influence with $\phi(\zeta)$. Physically, an increase in Nb improves the random motion of nanoparticles, which, in turn, lowers the concentration of nanofluid. Figure 10 shows that $\phi(\zeta)$ increases when Nt is increased.

The effect of various parameters on the local Nusselt number for $n = 0.7$ and 1.7 is studied using Table 2. The increment/decrement rate denotes the percentage change of the current

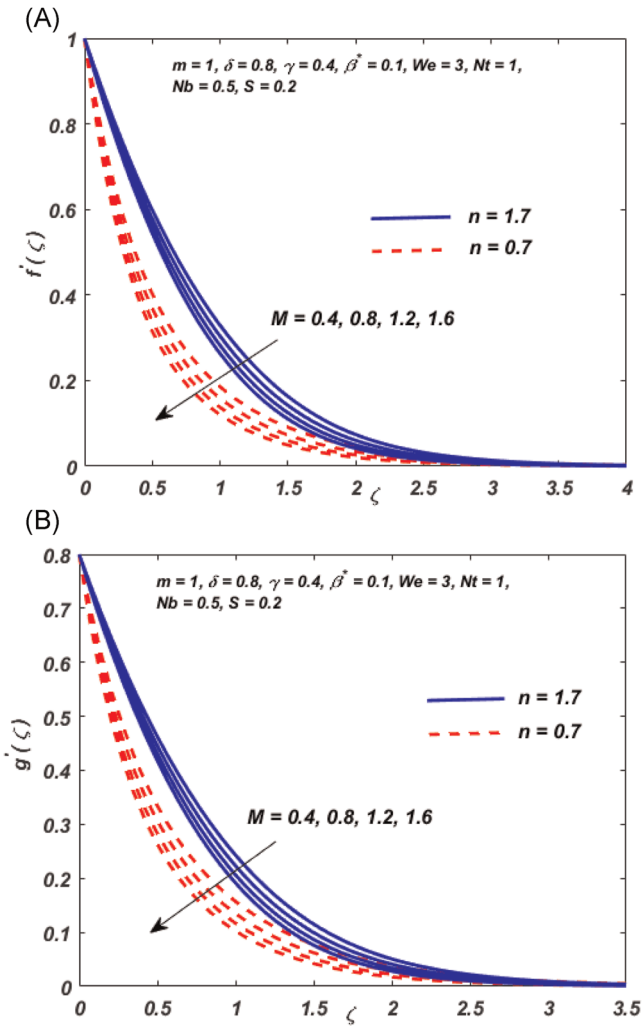

FIGURE 4 (A) Variation of $f'(\zeta)$ for various values of M and (B) variation of $g'(\zeta)$ for various values of M [Color figure can be viewed at wileyonlinelibrary.com]

value with respect to the previous value of the local Nusselt number. A positive sign represents an increment, whereas a negative sign represents a decrement in the heat transfer rate. From Table 2, it is deduced that $Re_x^{-\frac{1}{2}}Nu$ (both cases) increases with δ and decreases for Nt, S, and M. It is further noted that $Re_x^{-\frac{1}{2}}Nu$ $(n = 0.7)$ increases with β^* and decreases with We, whereas the results are reversed for $Re_x^{-\frac{1}{2}}Nu(n = 1.7)$. The slope of linear regression is used to study the trend of variation in the skin friction coefficient. A negative slope with respect to a parameter indicates that the parameter has a negative effect on skin friction, implying that an increase in that parameter will diminish the surface drag. The magnitude of slope represents the rate of change of the skin friction coefficient per unit value of the corresponding parameter. The impact of various parameters on skin friction coefficients for $m = 1$ and 3 at $n = 0.7$ and 1.7 is illustrated in Tables 3 and 4.

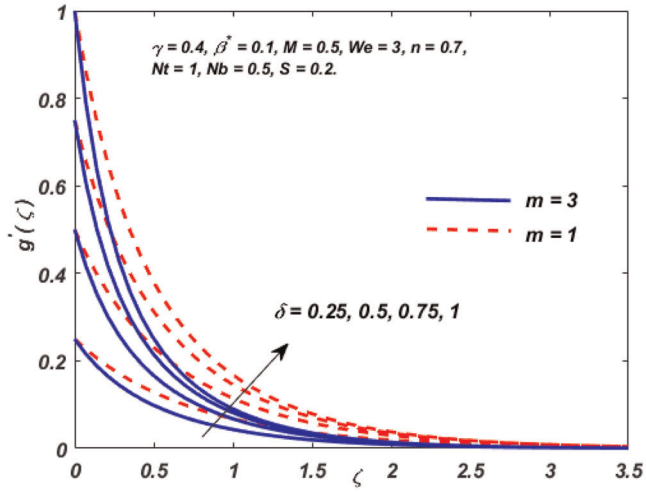

FIGURE 5 Variation of $g'(\zeta)$ for various values of δ [Color figure can be viewed at wileyonlinelibrary.com]

From Tables 3 and 4, it is inferred that *We* has a positive and negative impact on both skin friction coefficients $\{Re_x^{\frac{1}{2}}Cf_x$ and $Re_y^{\frac{1}{2}}Cf_y\}$ $(m = 1$ and $3)$ when $n = 0.7$ and 1.7, respectively, and β^* has a reverse impact on skin friction coefficients when compared with *We*. It is observed that M has a reducing effect on the surface drag. It is also observed that the skin friction coefficient decreases with increasing δ (for $Re_x^{\frac{1}{2}}Cf_x$) and increases with increasing δ (for $Re_y^{\frac{1}{2}}Cf_y$). The respective rate of change (slope) for each parameter is shown in Tables 3 and 4.

5 | STATISTICAL ANALYSIS

Statistical techniques, like, correlation and regression, are widely used by researchers to identify the nature of impact of independent variables (various parameters) on the dependent variable (physical quantities, like, Nusselt number, drag coefficient, or Sherwood number). The

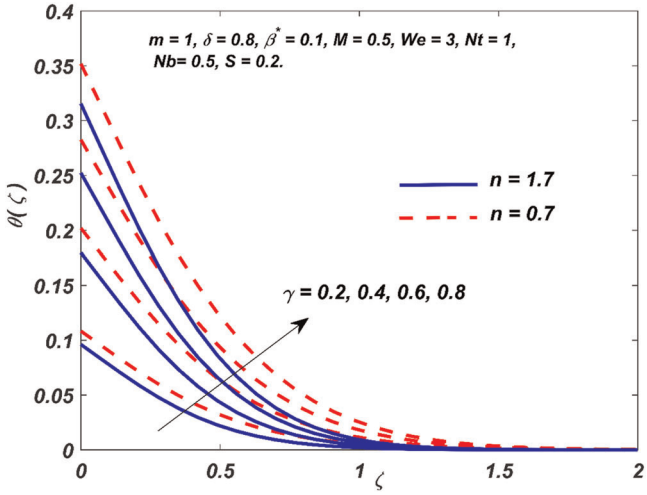

FIGURE 6 Variation of $\theta(\zeta)$ for various values of γ [Color figure can be viewed at wileyonlinelibrary.com]

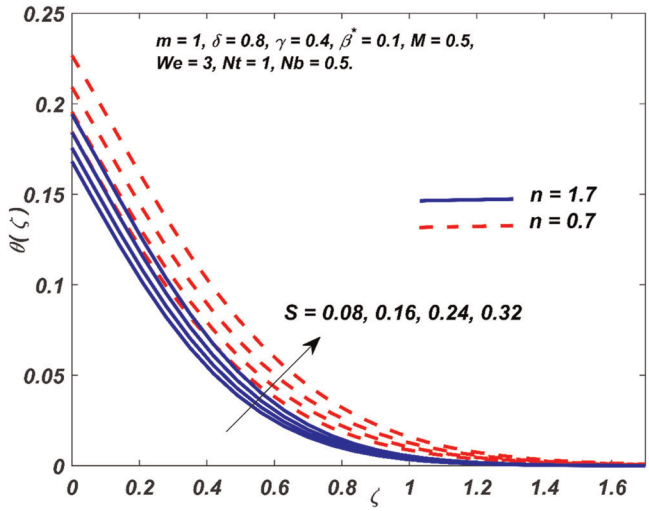

FIGURE 7 Variation of $\theta(\zeta)$ for various values of S [Color figure can be viewed at wileyonlinelibrary.com]

regression analysis helps in quantifying the variation of dependent variable due to the change in independent variables. It eliminates the need for solving the problem repeatedly, thereby simplifying the calculation process. An approximate value of dependent variable can be faultlessly predicted for the chosen range of independent variables.

5.1 | Correlation and probable error

Correlation is a statistical technique which helps in determining the degree of relationship between two variables. The sign of correlation coefficient (r) determines the nature of relationship, whereas the magnitude of r indicates the magnitude of the relationship.

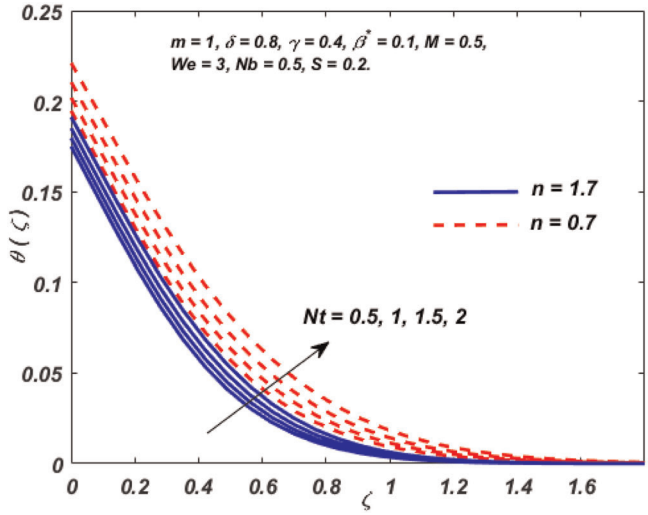

FIGURE 8 Variation of $\theta(\zeta)$ for various values of Nt [Color figure can be viewed at wileyonlinelibrary.com]

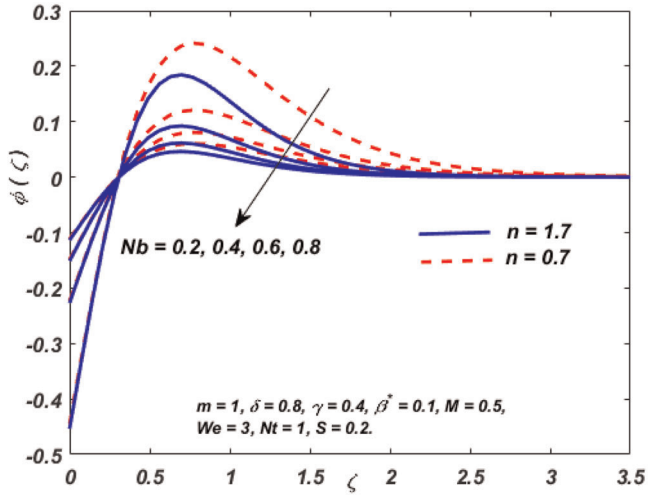

FIGURE 9 Variation of $\phi(\zeta)$ for various values of Nb [Color figure can be viewed at wileyonlinelibrary.com]

A positive value of the correlation coefficient implies that an increase in independent variable will fuel an increase in the dependent variable, and a negative value of the correlation coefficient indicates that an increase in independent variable will reduce the dependent variable. The reliability of the calculated correlation coefficient values is guaranteed using probable error (PE). Correlation is said to be significant[34] if $\left|\frac{r}{PE}\right| > 6$, where $PE = \left(\frac{1-r^2}{\sqrt{\varepsilon}}\right)0.6745$ and ε is the number of observations.

From Table 5, it is inferred that $Re_x^{-\frac{1}{2}}Nu$ (both cases) is positively correlated with δ and negatively correlated with S, M, and Nt. It is observed that We exhibits a negative and β^* exhibits a positive correlation for $Re_x^{-\frac{1}{2}}Nu(n = 0.7)$. It is also noted that the nature of correlation for We and β^* is reversed when $Re_x^{-\frac{1}{2}}Nu(n = 1.7)$. Using $\left|\frac{r}{PE}\right|$ values, it can be concluded that all parameters of $Re_x^{-\frac{1}{2}}Nu$ (both cases) are significant.

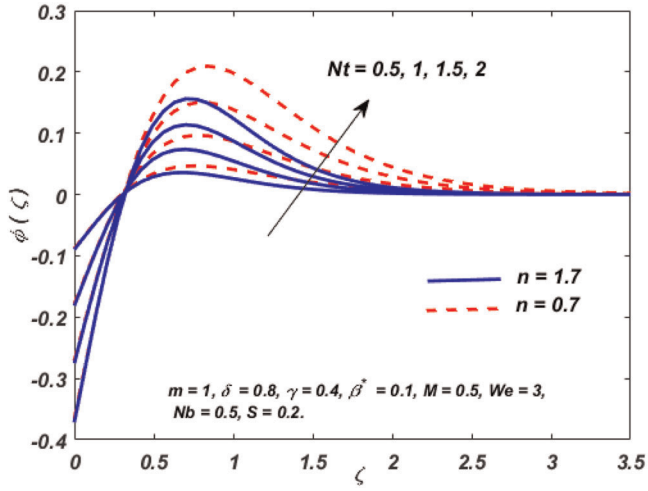

FIGURE 10 Variation of $\phi(\zeta)$ for various values of Nt [Color figure can be viewed at wileyonlinelibrary.com]

TABLE 2 Variation in the local Nusselt number at $\zeta = 0$ when $m = 1, Nt = 1, S = 0.2, M = 0.5, We = 3, \delta = 0.8, \beta^* = 0.1, Nb = 0.5$, and $\gamma = 0.4$

						$Re_x^{-\frac{1}{2}}Nu$		Increment/decrement rate	
Nt	***S***	***M***	δ	***We***	β^*	$n = 0.7$	$n = 1.7$	$n = 0.7$ (%)	$n = 1.7$ (%)
0.5						0.3220801	0.3299969		
0.875						0.3199708	0.3286018	−0.655	−0.423
1.25						0.3175703	0.3270705	−0.750	−0.466
1.625						0.3147927	0.325376	−0.875	−0.518
2						0.3115088	0.3234827	−1.043	−0.582
	0.08					0.3262050	0.3327401		
	0.14					0.3229700	0.3305449	−0.992	−0.660
	0.2					0.3192066	0.3281077	−1.165	−0.737
	0.26					0.3147406	0.3253792	−1.399	−0.832
	0.32					0.3092984	0.3222934	−1.729	−0.948
		0.4				0.3198040	0.3282712		
		0.7				0.3180105	0.3277891	−0.561	−0.147
		1				0.3162062	0.3273291	−0.567	−0.140
		1.3				0.3143798	0.3268877	−0.578	−0.135
		1.6				0.3125207	0.3264619	−0.591	−0.130
			0.25			0.2972953	0.3094536		
			0.4375			0.3071497	0.3172612	3.315	2.523
			0.625			0.3141479	0.3234272	2.278	1.944
			0.8125			0.3195285	0.3284102	1.713	1.541
			1			0.3238713	0.3325305	1.359	1.255
				2		0.3204980	0.3271069		
				3.5		0.3186733	0.3284715	−0.569	0.417
				5		0.3173661	0.3292629	−0.410	0.241
				6.5		0.3163448	0.3297959	−0.322	0.162
				8		0.3155017	0.3301881	−0.266	0.119
					0.1	0.3192066	0.3281077		
					0.3	0.3205573	0.3276043	0.423	−0.153
					0.5	0.3216038	0.3269473	0.326	−0.201
					0.7	0.3224475	0.3260304	0.262	−0.280
					0.9	0.3231473	0.3245935	0.217	−0.441

TABLE 3 Variation in skin friction coefficients at $\zeta = 0$ when $m = 1, Nt = 1, S = 0.2, M = 0.5, We = 3, \delta = 0.8, \beta^* = 0.1, Nb = 0.5$, and $\gamma = 0.4$

				$-Re_x^{\frac{1}{2}} Cf_x$		$-Re_y^{\frac{1}{2}} Cf_y$	
We	β^*	***M***	δ	$n = 0.7$	$n = 1.7$	$n = 0.7$	$n = 1.7$
2				1.33511	1.86889	1.52449	2.02782
4				1.22088	2.15347	1.39943	2.32086
6				1.15550	2.36256	1.32533	2.54024
8				1.11123	2.52993	1.27460	2.71707
Slope				**−0.03685**	**0.10961**	**−0.04119**	**0.11436**
	0.2			1.30295	1.98544	1.48571	2.14815
	0.4			1.36500	1.90031	1.54612	2.06399
	0.6			1.42028	1.80114	1.60037	1.96670
	0.8			1.47045	1.67999	1.64987	1.84939
Slope				**0.27889**	**−0.50776**	**0.27337**	**−0.49678**
		0.4		1.24376	1.97236	1.42361	2.13213
		0.8		1.33935	2.17465	1.53495	2.34492
		1.2		1.42665	2.36590	1.63649	2.54627
		1.6		1.50737	2.54804	1.73028	2.73812
Slope				**0.21953**	**0.47958**	**0.25539**	**0.50483**
			0.25	1.12977	1.70474	2.51655	2.89424
			0.5	1.19716	1.84841	1.81195	2.36941
			0.75	1.25722	1.99478	1.49662	2.20445
			1	1.31215	2.14103	1.31215	2.14103
Slope				**0.24288**	**0.58209**	**−1.57142**	**−0.96983**

Note: The bold values denote the slope of linear regression.

5.2 | Multiple linear regression

The regression analysis is a statistical modeling technique used to establish a relationship between a dependent (Nusselt number) and one or more independent (various parameters considered) variables. The local Nusselt number for $n = 0.7$ and 1.7 is estimated using multiple linear regression models (as all correlations are significant). The estimated models are as follows:

$$Nu_{\text{est}}^{n=0.7} = r_S S + r_M M + r_\delta \delta + r_{We} We + r_{\beta^*} \beta^* + r_{Nt} Nt + c,$$

$$Nu_{\text{est}}^{n=1.7} = r_S S + r_M M + r_\delta \delta + r_{We} We + r_{\beta^*} \beta^* + r_{Nt} Nt + c,$$

where r_S, r_M, r_δ, r_{We}, r_{β^*}, r_{Nt}, and c are the estimated regression coefficients.

$Re_x^{-\frac{1}{2}} Nu$ is estimated from 30 sets of values chosen in the range [0.08,0.32] for S, [0.4,1.6] for M, [0.25,1] for δ, [2,8] for We, [0.1,0.9] for β^*, and [0.5,2] for Nt, and the regression

TABLE 4 Variation in skin friction coefficients at $\zeta = 0$ when $m = 3, Nt = 1, S = 0.2, M = 0.5, We = 3, \delta = 0.8, \beta^* = 0.1, Nb = 0.5$, and $\gamma = 0.4$

				$-Re_x^{\frac{1}{2}} Cf_x$		$-Re_y^{\frac{1}{2}} Cf_y$	
We	**β^***	**M**	**δ**	**$n = 0.7$**	**$n = 1.7$**	**$n = 0.7$**	**$n = 1.7$**
2				1.91894	3.05400	2.19540	3.30479
4				1.74778	3.56384	2.00299	3.83948
6				1.65419	3.92644	1.89571	4.22410
8				1.59169	4.21322	1.82361	4.52954
Slope				**−0.05377**	**0.19201**	**−0.06113**	**0.20294**
	0.2			1.88497	3.25976	2.14958	3.52184
	0.4			2.00493	3.09201	2.27040	3.35199
	0.6			2.11052	2.89401	2.37747	3.15268
	0.8			2.20561	2.64641	2.47432	2.90610
Slope				**0.53376**	**−1.01903**	**0.54065**	**−1.02327**
		0.4		1.80207	3.29733	2.06412	3.55888
		0.8		1.86302	3.44808	2.13524	3.71650
		1.2		1.92130	3.59477	2.20316	3.87005
		1.6		1.97723	3.73779	2.26826	4.01989
Slope				**0.14593**	**0.36702**	**0.17009**	**0.38415**
			0.25	1.58658	2.71252	3.59345	4.50058
			0.5	1.69935	2.99380	2.58371	3.81117
			0.75	1.79885	3.27865	2.14315	3.61699
			1	1.88932	3.56095	1.88932	3.56095
Slope				**0.40309**	**1.13206**	**−2.22118**	**−1.20522**

Note: The bold values denote the slope of linear regression.

TABLE 5 Correlation coefficient (r), probable error (PE), and $\left|\frac{r}{PE}\right|$ of the reduced Nusselt number at $\zeta = 0$ when $\gamma = 0.4$ and $Nb = 0.5$

	$Re_x^{-\frac{1}{2}} Nu$ when $n = 0.7$			$Re_x^{-\frac{1}{2}} Nu$ when $n = 1.7$		
Parameter	**r**	**PE**	$\left\|\frac{r}{PE}\right\|$	**r**	**PE**	$\left\|\frac{r}{PE}\right\|$
S	−0.9947	0.0032	311.6281	−0.9977	0.0014	732.2152
M	−1	0	63550.2092	−0.9997	0.0002	5508.9911
δ	0.9866	0.0080	122.7986	0.9920	0.0048	207.3562
We	−0.9879	0.0072	136.5306	0.9689	0.0185	52.4026
β*	0.9915	0.0051	194.3342	−0.9780	0.0131	74.4632
Nt	−0.9962	0.0023	430.4705	−0.9982	0.0011	909.9878

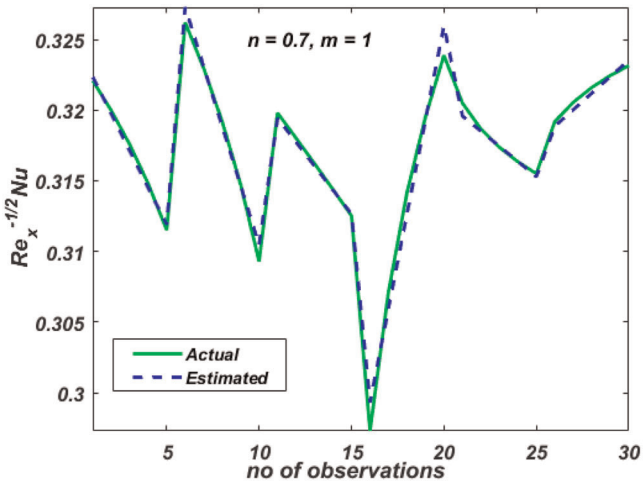

FIGURE 11 Actual and estimated values of $Re_x^{-\frac{1}{2}}Nu$ when $n = 0.7$ [Color figure can be viewed at wileyonlinelibrary.com]

coefficients are calculated using MATLAB software. As the p values for all physical parameters are less than 0.05, the regression coefficients are significant. A positive regression coefficient represents that the corresponding parameter has an increasing effect on the local Nusselt number, and a negative regression coefficient implies that the local Nusselt number decreases with respect to the corresponding parameter. The estimated regression models are expressed as follows:

$$Nu_{\text{est}}^{n=0.7} = -0.07007S - 0.00566M + 0.03556\delta - 0.00072We + 0.00583\beta^* - 0.00697Nt + 0.31579,$$

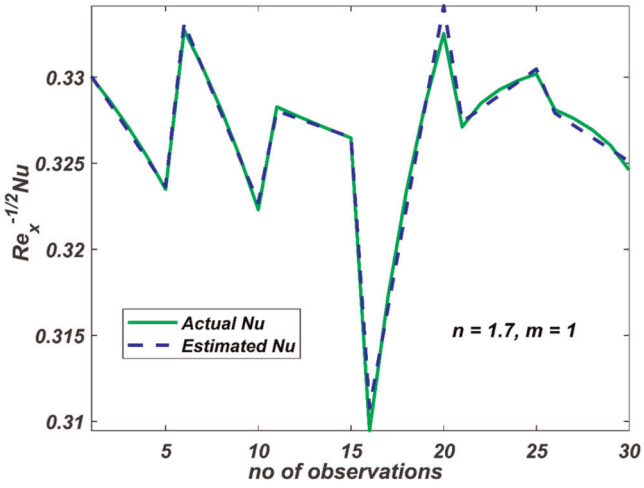

FIGURE 12 Actual and estimated values of $Re_x^{-\frac{1}{2}}Nu$ when $n = 1.7$ [Color figure can be viewed at wileyonlinelibrary.com]

$$Nu_{\text{est}}^{n=1.7} = -0.04343S - 0.00128M + 0.03116\delta + 0.00051We - 0.00352\beta^* - 0.00428Nt + 0.31540.$$

The accuracy of the estimated regression model is illustrated using Figures 11 and 12. It is conclusive that δ and β^* have a positive impact and S, M, We, and Nt have a negative impact on the Nusselt number when $n = 0.7$. It can also be concluded that δ and We have a positive impact and S, M, β^*, and Nt have a negative impact on the Nusselt number when $n = 1.7$. This is in agreement with the results seen in Table 2.

6 | CONCLUDING REMARKS

The major conclusions drawn from the current analysis are as follows:

- The velocity profiles are directly proportional to the viscosity ratio parameter in the shear-thinning case and inversely proportional in the shear-thickening case.
- The Weissenberg number enhances the velocity profiles in case of shear-thickening fluids and retards the velocity profiles for shear-thinning fluids.
- An exponential increase is observed in the temperature profile due to an increase in the Biot number, heat generation/absorption, and thermophoresis parameters.
- The Hartmann number has a destructive effect on surface drag and the velocity profiles.
- An increase in the stretching ratio parameter improves the Y-directional velocity profile.
- The concentration profile is enhanced and depleted with an increase in thermophoresis and Brownian motion effects, respectively.
- The regression models are found to be in synchronization with the numerical results for the chosen values of parameters.

ACKNOWLEDGMENT

The authors acknowledge learned reviewers for their thoughtful comments and constructive suggestions.

CONFLICT OF INTERESTS

The authors declare that there is no conflict of interests.

NOMENCLATURE

a, b, m	constants
B_0	strength of magnetic field
C	fluid concentration (moles/kg)
C_{W}	nanoparticle concentration near the wall (moles/kg)
C_∞	ambient nanoparticle concentration (moles/kg)
D_{B}	Brownian diffusion coefficient ($\text{m}^2\,\text{s}^{-1}$)
D_{T}	thermophoretic diffusion coefficient ($\text{m}^2\,\text{s}^{-1}$)
$f'(\zeta), g'(\zeta)$	velocity components
h_{f}	convective heat transfer coefficient ($\text{W}\,\text{K}^{-1}\,\text{m}^{-2}$)
H	Hartmann number
k_{f}	thermal conductivity of fluid ($\text{W}\,\text{m}^{-1}\,\text{K}^{-1}$)
n	power-law index

Nb	Brownian motion parameter
Nt	thermophoresis parameter
Nu	Nusselt number
Pr	Prandtl number
Q_0	intensity of heat source
Re_x	local Reynolds number
S	heat generation/absorption parameter
Sc	Schmidt number
T	fluid temperature (K)
T_W	temperature of the fluid near the wall (K)
T_∞	temperature of the ambient fluid (K)
u, v, w	velocity components (m/s)
u_W, v_W	stretching velocities (m/s)
We	local Weissenberg number
x, y, z	Cartesian coordinates

GREEK SYMBOLS

α	thermal diffusivity ($m^2\,s^{-1}$)
β^*	viscosity ratio parameter
δ	stretching ratio parameter
γ	Biot number
Γ	time material constant (s)
ν	kinematic viscosity ($m^2\,s^{-1}$)
ϕ	dimensionless concentration
ρ	density ($kg\,m^{-3}$)
$(\rho C)_f$	heat capacity of the fluid
σ	electrical conductivity
τ	effective heat capacity ratio
θ	dimensionless temperature
ζ	dimensionless variable

SUBSCRIPTS

f fluid
w condition at the wall

ORCID

Sujesh Areekara http://orcid.org/0000-0001-7860-8268
Alphonsa Mathew http://orcid.org/0000-0002-3810-4484

REFERENCES

1. Vinita V, Poply V. Impact of outer velocity MHD slip flow and heat transfer of nanofluid past a stretching cylinder. *Mater Today Proc*. 2019;26(3):3429-3435. https://doi.org/10.1016/j.matpr.2019.11.304
2. Rabbi KM, Sheikholeslami M, Karim A, Shafee A, Li Z, Tlili I. Prediction of MHD flow and entropy generation by artificial neural network in square cavity with heater-sink for nanomaterial. *Phys A: Stat Mech Appl*. 2020;541:123520. https://doi.org/10.1016/j.physa.2019.123520

3. Sulaiman Alsagri A, Hassanpour A, Alrobaian AA. Simulation of MHD nanofluid flow in existence of viscous dissipation by means of ADM. *Case Stud Therm Eng*. 2019;14:100494. https://doi.org/10.1016/j.csite.2019.100494
4. Naga Santoshi P, Venkata Ramana Reddy G, Padma P. Numerical Study of Carreau Nanofluid Flow Under Slips. *Int J Appl Comput Math*. 2019;5. https://doi.org/10.1007/s40819-019-0706-z
5. Abbas T, Rehman S, Shah RA, Idrees M, Qayyum M. Analysis of MHD Carreau fluid flow over a stretching permeable sheet with variable viscosity and thermal conductivity. *Phys A: Stat Mech Appl*. 2020;551:124225. https://doi.org/10.1016/j.physa.2020.124225
6. Goudarzi S, Shekaramiz M, Omidvar A, Golab E, Karimipour A, Karimipour A. Nanoparticles migration due to thermophoresis and Brownian motion and its impact on Ag–MgO/water hybrid nanofluid natural convection. *Powder Technol*. 2020;375:493-503. https://doi.org/10.1016/j.powtec.2020.07.115
7. Sardar H, Ahmad L, Khan M, Alshomrani AS. Investigation of mixed convection flow of Carreau nanofluid over a wedge in the presence of Soret and Dufour effects. *Int J Heat Mass Transfer*. 2019;137:809-822. https://doi.org/10.1016/j.ijheatmasstransfer.2019.03.132
8. Hayat T, Qayyum S, Alsaedi A, Shafiq A. Theoretical aspects of Brownian motion and thermophoresis on nonlinear convective flow of magneto Carreau nanofluid with Newtonian conditions. *Results Phys*. 2018;10:521-528. https://doi.org/10.1016/j.rinp.2018.04.027
9. Iqbal K, Ahmed J, Khan M, Ahmad L, Alghamdi M. Magnetohydrodynamic thin film deposition of Carreau nanofluid over an unsteady stretching surface. *Appl Phys A: Mater Sci Process*. 2020;126:1-13. https://doi.org/10.1007/s00339-019-3204-6
10. Khan JA, Mustafa M, Hayat T, Alsaedi A. On three-dimensional flow and heat transfer over a non-linearly stretching sheet: analytical and numerical solutions. *PLOS ONE*. 2014;9:1-11. https://doi.org/10.1371/journal.pone.0107287
11. Hussain Z, Hayat T, Alsaedi A, Ahmad B. Three-dimensional convective flow of CNTs nanofluids with heat generation/absorption effect: a numerical study. *Comput Methods Appl Mech Eng*. 2017;329:40-54. https://doi.org/10.1016/j.cma.2017.09.026
12. Nandeppanavar MM, Siddalingappa MN. Effect of viscous dissipation and thermal radiation on heat transfer over a non-linearly stretching sheet through porous medium. *Int J Appl Mech Eng*. 2013;18:461-474. https://doi.org/10.2478/ijame-2013-0027
13. Tlili I, Bilal M, Qureshi M, Abdelmalek Z. Thermal analysis of magnetized pseudoplastic nano fluid flow over 3D radiating non-linear surface with passive mass flux control and chemically responsive species. *J Mater Res Technol*. 2020;9:8125-8135. https://doi.org/10.1016/j.jmrt.2020.05.073
14. Hayat T, Aziz A, Muhammad T, Alsaedi A. Numerical simulation for three-dimensional flow of Carreau nanofluid over a nonlinear stretching surface with convective heat and mass conditions. *J Braz Soc Mech Sci Eng*. 2019;7:1-11. https://doi.org/10.1007/s40430-018-1540-7
15. Shakunthala S, Nandeppanavar MM. Boundary layer flow and Cattaneo–Christov heat flux of a nonlinear stretching sheet with a suspended CNT. *Nanosci Nanotechnol—Asia*. 2019;9:494-503. https://doi.org/10.2174/2210681208666180821142231
16. Patel HR, Singh R. Thermophoresis, Brownian motion and non-linear thermal radiation effects on mixed convection MHD micropolar fluid flow due to nonlinear stretched sheet in porous medium with viscous dissipation, Joule heating and convective boundary condition. *Int Commun Heat Mass Transfer*. 2019;107:68-92. https://doi.org/10.1016/j.icheatmasstransfer.2019.05.007
17. Tlili I, Hamadneh NN, Khan WA. Thermodynamic analysis of MHD heat and mass transfer of nanofluids past a static wedge with Navier slip and convective boundary conditions. *Arab J Sci Eng*. 2018;44:1255-1267. https://doi.org/10.1007/s13369-018-3471-0
18. Nayak MK, Shaw S, Pandey VS, Chamkha AJ. Combined effects of slip and convective boundary condition on MHD 3D stretched flow of nanofluid through porous media inspired by non-linear thermal radiation. *Indian J Phys*. 2018;92:1017-1028. https://doi.org/10.1007/s12648-018-1188-2
19. Ray AK, Vasu B, Murthy PVSN, Gorla RSR. Non-similar solution of Eyring–Powell fluid flow and heat transfer with convective boundary condition: homotopy analysis method. *Int J Appl Comput Math*. 2020;6:16. https://doi.org/10.1007/s40819-019-0765-1

20. Kuznetsov AV, Nield DA. The Cheng–Minkowycz problem for natural convective boundary layer flow in a porous medium saturated by a nanofluid: a revised model. *Int J Heat Mass Transfer*. 2013;65:682-685. https://doi.org/10.1016/j.ijheatmasstransfer.2013.06.054
21. Ul Haq R, Nadeem S, Hayat Khan Z, Sher Akbar N. Thermal radiation and slip effects on MHD stagnation point flow of nanofluid over a stretching sheet. *Phys E: Low-Dimensional Syst Nanostruct*. 2015;65:17-23. https://doi.org/10.1016/j.physe.2014.07.013
22. Ramzan M, Sheikholeslami M, Saeed M, Chung JD. On the convective heat and zero nanoparticle mass flux conditions in the flow of 3D MHD couple stress nanofluid over an exponentially stretched surface. *Sci Reports*. 2019;9:1-13. https://doi.org/10.1038/s41598-018-37267-2
23. Uddin I, Altaf M, Ullah S, Islam S, Israr M, Hussain F. Characteristics of buoyancy force on stagnation point flow with magneto-nanoparticles and zero mass flux condition. *Results Phys*. 2018;8:160-168. https://doi.org/10.1016/j.rinp.2017.10.038
24. Saif-ur-Rehman NAMir, Farooq M, Rizwan M, Ahmad F, Ahmad S, Ahmad B. Analysis of thermally stratified flow of Sutterby nanofluid with zero mass flux condition. *J Mater Res Technol*. 2020;9:1631-1639. https://doi.org/10.1016/j.jmrt.2019.11.088
25. Hayat T, Ahmed B, Alsaedi A, Abbasi FM. Numerical study for peristalsis of Carreau–Yasuda nanomaterial with convective and zero mass flux condition. *Results Phys*. 2018;8:1168-1177. https://doi.org/10.1016/j.rinp.2017.12.070
26. Khan M, Azam M, Alshomrani AS. Unsteady slip flow of Carreau nanofluid over a wedge with nonlinear radiation and new mass flux condition. *Results Phys*. 2017;7:2261-2270. https://doi.org/10.1016/j.rinp.2017.06.038
27. Nandeppanavar M, Kemparaju M, Shilpa J. Heat and mass transfer analysis of Carreau nanofluid over an exponentially stretching sheet in a saturated porous medium. *J Nanofluids*. 2018;8:990-997. https://doi.org/10.1166/jon.2019.1656
28. Khan M, Hussain A, Malik MY, Salahuddin T, Aly S. Numerical analysis of Carreau fluid flow for generalized Fourier's and Fick's laws. *Appl Numer Math*. 2019;144:100-117. https://doi.org/10.1016/j.apnum.2019.05.018
29. Mackolil J, Mahanthesh B. Exact and statistical computations of radiated flow of nano and Casson fluids under heat and mass flux conditions. *J Comput Des Eng*. 2019;6:593-605. https://doi.org/10.1016/j.jcde.2019.03.003
30. Mahanthesh B, Mackolil J, Shehzad SA. Statistical analysis of stagnation—point heat flow in Williamson fluid with viscous dissipation and exponential heat source effects. *Heat Transfer*. 2020;49(8):4580-4591. https://doi.org/10.1002/htj.21842
31. Mahanthesh B, Shankarappa N, Jayanna B, Lare I. Effectiveness of Hall current and exponential heat source on unsteady heat transport of dusty TiO_2-EO nanoliquid with nonlinear radiative heat. *J Comput Des Eng*. 2019;6:551-561. https://doi.org/10.1016/j.jcde.2019.04.005
32. Khan M, Sardar H, Hashim. Heat generation/absorption and thermal radiation impacts on three-dimensional flow of Carreau fluid with convective heat transfer. *J Mol Liq*. 2018;272:474-480. https://doi.org/10.1016/j.molliq.2018.08.088
33. Mahanthesh B, Gireesha BJ, Subba R, Gorla R. Unsteady three-dimensional MHD flow of a nano Eyring–Powell fluid past a convectively heated stretching sheet in the presence of thermal radiation, viscous dissipation and Joule heating. *J Assoc Arab Univ Basic Appl Sci*. 2017;23:75-84. https://doi.org/10.1016/j.jaubas.2016.05.004
34. Fisher R. On the "Probable Error" of a coefficient of correlation deduced from a small sample. *Metron*. 1921;1:1-32. https://ci.nii.ac.jp/naid/10012392243/en/

How to cite this article: Sabu AS, Areekara S, Mathew A. Statistical analysis on three-dimensional MHD convective Carreau nanofluid flow due to bilateral nonlinear stretching sheet with heat source and zero mass flux condition. *Heat Transfer*. 2021;50:3641–3660. https://doi.org/10.1002/htj.22045